Hot-Carrier Degradation in Single-Layer Double-Gated Graphene Field-Effect Transistors

Yu.Yu. Illarionov*†, M. Waltl*, A.D. Smith‡, S. Vaziri‡, M. Ostling‡, T. Mueller§, M.C. Lemme¶ and T. Grasser*

* Institute for Microelectronics, TU Wien, Austria
† Ioffe Physical-Technical Institute, Russia
‡ KTH Royal Institute of Technology, Sweden
§ Institute for Photonics, TU Wien, Austria
¶ University of Siegen, Germany

***Abstract*—We report a first study of hot-carrier degradation (HCD) in graphene field-effect transistors (GFETs). Our results show that HCD in GFETs is recoverable, similarly to the bias-temperature instability (BTI). Depending on the top gate bias polarity, the presence of HCD may either accelerate or suppress BTI. Contrary to BTI, which mainly results in a change of the charged trap density in the oxide, HCD also leads to a mobility degradation which strongly correlates with the magnitude of the applied stress.**

I. Introduction

Graphene is a next-generation carbon material which is characterized by outstanding physical and electrical properties [1, 2] and has a good compatibility with standard complimentary metal oxide semiconductor (CMOS) technology [3]. Therefore, it can be considered as a promising material for advanced electronic devices that could enhance the performance or functionality of silicon integrated circuits. Since the discovery of the field effect in graphene [4], several research groups have succeeded in fabricating graphene-based FETs (GFETs) [5–7]. However, only a few attempts have been made at trying to understand their reliability [8–10]. All these previous works are devoted to bias-temperature instabilities (BTI) but no analysis has been attempted with respect to hot-carrier degradation (HCD), which is another key reliability issue in Si technologies [11]. We thus perform a detailed study of HCD in the high-k top gate of double-gated GFETs and analyze the dependence of the degradation/recovery dynamics on the magnitude and polarity of the applied stress.

II. Devices

Double-gated GFETs with the graphene channel sandwiched between Al_2O_3 (top gate) and SiO_2 (back gate) were fabricated on a thermally oxidized Si substrate using a standard contact lithography process [3]. Their isometric view and schematic cross-section are given in Fig. 1. In the spirit of the standard forming-gas anneal of Si technology [12], the devices have been treated by baking at $T = 300^{\circ}$C in an H_2/He mixture, which allowed us to reach a significant decrease in variability [13]. As shown in our previous works [10, 13], our GFETs demonstrate all typical properties known from literature reports [8].

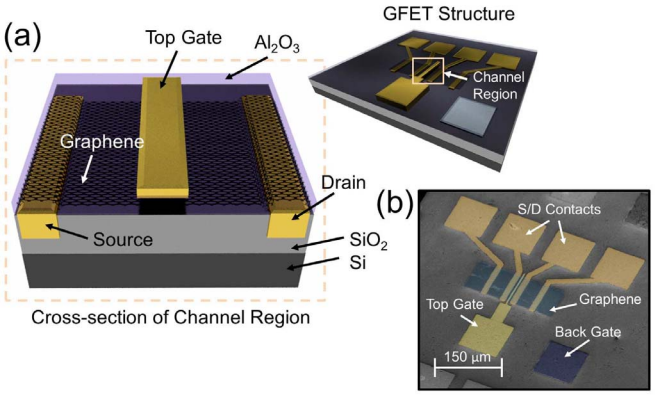

Fig. 1: a) Schematic layout of the double-gated single-layer GFET and a cross-section of the channel region ($L = 4\,\mu$m and $W = 20$–$80\,\mu$m). b) Top view of the double-gated GFET obtained using scanning-electron microscopy (SEM). The top gates are made of TiAu and the back gates of Al.

III. Experiment

Our studies are based on the analysis of the transformation of the top gate transfer characteristics of GFETs which are known to be sensitive to the detrimental impact of the environment [9]. For this reason, all our measurements were performed in vacuum (10^{-5} torr). The impact of HCD and bias stress on the device performance was examined as follows: after measuring the reference transfer characteristic, a stress with constant V_{TG} and drain voltage V_d was applied for a certain time; the back gate bias V_{BG} was set to zero and V_d was positive all the time (i.e. pHCD). Then the recovery of the stressed device was monitored for several hours/days after which a new stress with either a larger stress time t_s or V_d was applied. Similarly to our previous work [13], V_{TG}-$V_D(t_s) \approx$ const with V_D being the Dirac voltage was maintained in order to approximately keep the oxide field constant during all stress rounds.

IV. Results and discussions

In Fig. 2 the resulting time evolution of the top gate transfer characteristics after HCD stress with the same $V_d = 5$ V and different V_{TG}-V_D is depicted. Clearly, even in the case of rather small negative V_{TG}-V_D (i.e. NBTI-HCD) the Dirac voltage is

978-1-4673-7362-3/15/$31.00 ©2015 IEEE

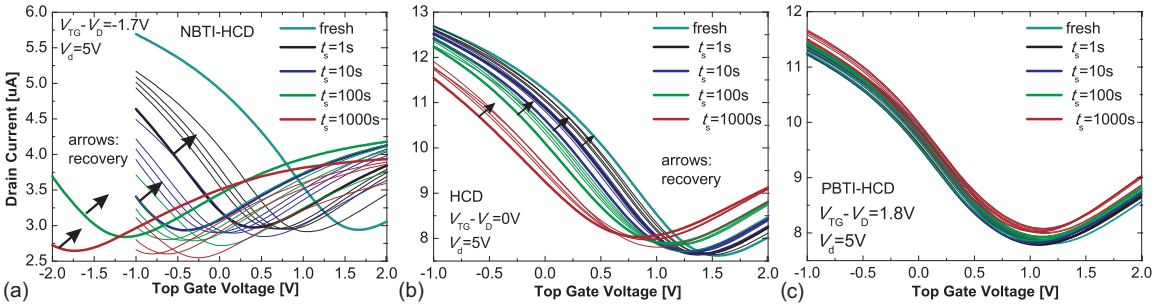

Fig. 2: Time evolution of the top gate transfer characteristics measured at 20mV drain bias after NBTI-HCD (a), pure HCD (b) and PBTI-HCD (c). Clearly, the HCD component having NBTI-like nature leads to a significant acceleration of NBTI degradation even if the applied negative V_{TG}-V_D is rather small. At the same time, the PBTI degradation caused by positive V_{TG}-V_D of the same absolute magnitude is almost completely compensated by the HCD component.

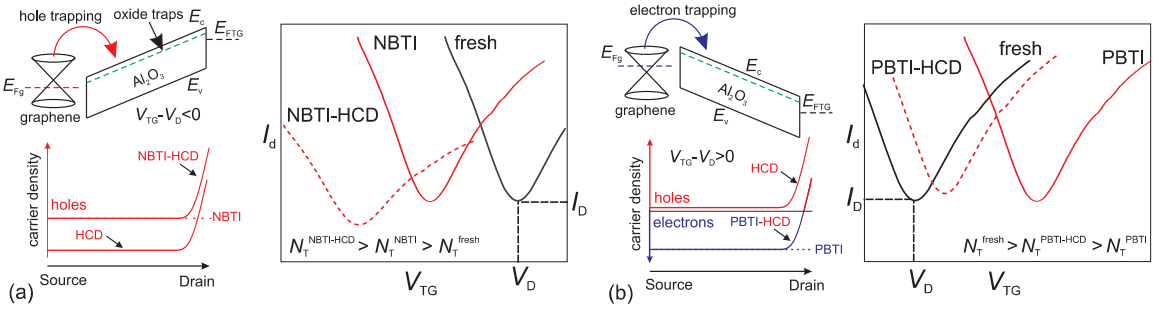

Fig. 3: a) Band diagram of the top gate cross-section of a GFET and a schematic evolution of the transfer characteristic in the case of V_{TG}-$V_D<0$ (NBTI-like stress). The holes are trapped by the oxide traps. Thus the density of positive trap charge N_T at the oxide/graphene interface increases and the Dirac voltage determined by -qN_T/C_{ox} is shifted towards more negative values (NBTI). The HCD component increases the density of holes near the drain, which leads to the creation of additional positively charged defects at the drain side of the channel (NBTI-HCD). Therefore, N_T further increases, i.e. NBTI is accelerated by HCD. In addition, other defects in graphene and gate oxides become charged and thus the carrier mobility and residual density change. This is reflected in a transformation of the shape and vertical drift of the transfer characteristics. b) Similar plots for V_{TG}-$V_D>0$ (PBTI-like stress). The electrons are transferred from graphene to the oxide and become trapped. Thus N_T decreases and the Dirac point is shifted towards more positive values (PBTI). The HCD component decreases the electron concentration near the drain and introduces extra holes. Therefore, creation of positively charged defects at the drain side of the channel becomes favourable. These positive defects partially compensate the negative charge introduced by PBTI and are situated mostly at the source side of the channel, making the V_D shift less pronounced (PBTI-HCD). At the same time, the shape of the characteristics is modified thus reflecting a mobility change.

significantly shifted towards more negative values and some vertical drift ΔI_D is observed (Fig. 2a). With the bias stress V_{TG}-V_D set to zero (Fig. 2b), the pure HCD component still shifts the Dirac point in an NBTI-like manner. Interestingly, in both cases the HCD degradation is recoverable, contrary to Si technologies. At the same time, a small positive V_{TG}-V_D (i.e. PBTI-HCD) accompanied by the HCD component has only a negligible impact on the transfer characteristics (Fig. 2c). Thus one can conclude that in our GFETs NBTI degradation is accelerated and PBTI is suppressed by the HCD component with positive drain bias. This behaviour can be understood based on the band diagrams given in Fig. 3. If a negative V_{TG}-V_D is applied (Fig. 3a), the holes are transferred from graphene and trapped by the oxide traps. As a result a density of positively charged states at the graphene/Al_2O_3 interface N_T increases which leads to an NBTI-like shift of the Dirac point. Thus an acceleration of NBTI degradation by the HCD component means that the latter creates additional positively charged defects closely to the drain and increases N_T. In the case of positive V_{TG}-V_D (Fig. 3b) the electrons from the graphene channel are trapped by oxide traps and thus N_T decreases which is associated with PBTI-like degradation. However, if a PBTI stress is applied in conjuction with HCD, the negatively charged defects situated mostly at the source side of the channel are partially compensated by the positively charged defects created by the HCD component closely to the drain. Therefore, the net decrease in N_T becomes smaller and PBTI is suppressed by the HCD component. Finally, we can conclude that while pure BTI results in a uniform distribution of the charges along the channel, the presence of HCD introduces a significant non-uniformity.

In Fig. 4 the results for NBTI-HCD with a large bias component V_{TG}-V_D=-6 V are shown. Contrary to Fig. 2a, the NBTI-like Dirac point shift ΔV_D increases versus the stress time only up to t_s=100 s while the subsequent stress rounds with longer t_s lead to a decrease in ΔV_D. For example, the ΔV_D recovery trace corresponding to t_s=10000 s lies even below the one for t_s=1 s (Fig. 4b). This indicates that all the defects are positively charged after t_s=100 s, and the next stress cycles lead to disappearing of some defects, similarly to Si technologies [14, 15]. This situation can be depicted in terms of the charged trap density shift $\Delta N_T = C_{ox}\Delta V_D/q$ which decreases at larger t_s (Fig. 4c). Interestingly, the longest stresses modify the characteristics more significantly which hints at mobility degradation. Also, it is obvious that independently of t_s the recovery traces (Fig. 4b) have some kinks associated with a fast trap component, similarly to pure NBTI in GFETs [13]. In Fig. 5 we reproduce the results for PBTI-HCD with V_{TG}-V_D=4 V and V_d=5 V. One can see that PBTI-like degradation is observed for all t_s and that

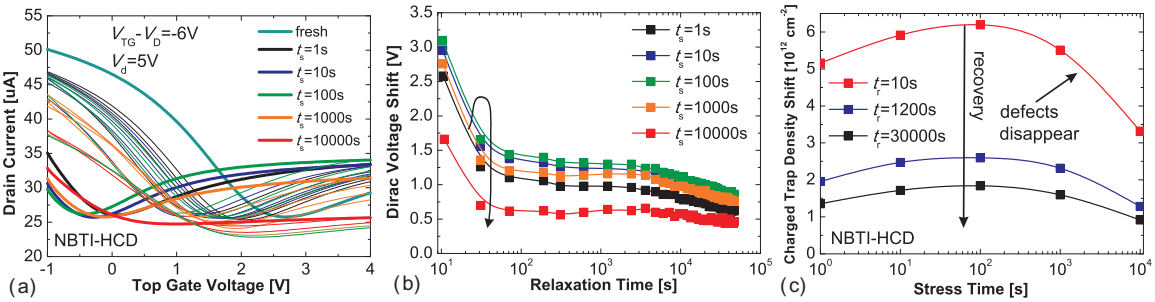

Fig. 4: a) Time evolution of the top gate transfer characteristics after NBTI-HCD stress with $V_{TG}-V_D=-6$ V and $V_d=5$ V. b) The corresponding recovery traces demonstrate that a significant increase of the Dirac voltage shift versus stress time takes place only up to $t_s=10$ s. The trace for $t_s=100$ s is only slightly above the one for $t_s=10$ s which indicates that all the defects are positively charged and thus a further increase of N_T is not possible. Subsequent stress cycles with larger t_s lead to a decrease in the Dirac voltage shift possibly, because defects disappear, similarly to Si technologies [14, 15]. c) This behaviour can be depicted in terms of the charged trap density shift $\Delta N_T=C_{ox}\Delta V_D/q$ which can be calculated at different recovery stages.

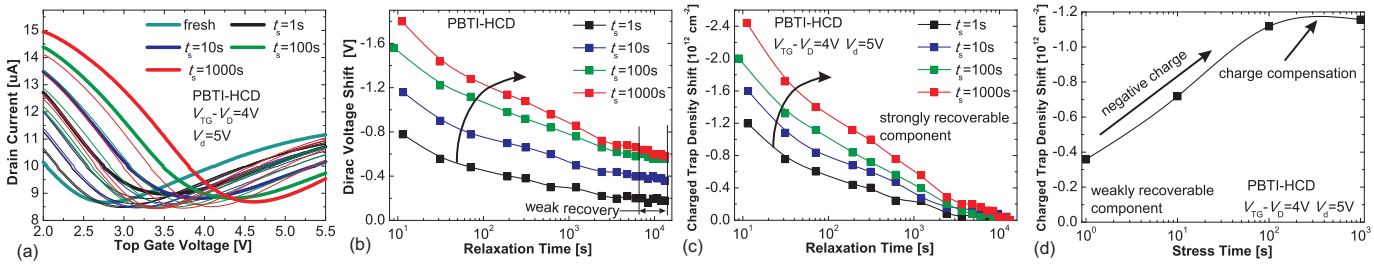

Fig. 5: a) Time evolution of the top gate transfer characteristics after PBTI-HCD stress with $V_{TG}-V_D=4$ V and $V_d=5$ V. b) The corresponding ΔV_D recovery traces demonstrate that the magnitude of PBTI-like degradation increases versus t_s, which means that a strong PBTI contribution dominates over the HC impact. The recovery traces contain both strongly recoverable (c) and weakly recoverable (d) components which can be represented in terms of a charged trap density shift. The strongly recoverable component is associated with a relaxation of negatively charged defects introduced by the PBTI contribution. Therefore, it becomes more pronounced for larger t_s, similarly to the case of a pure PBTI (cf. [13]). The presence of a weakly recoverable component leads to an incomplete recovery which is also due to the presence of negative charge introduced by the bias contribution. However, for larger t_s the weakly recoverable component tends to saturate, since the amount of positively charged defects created by the HC contribution becomes enough for partial compensation of negative charge introduced by the bias contribution. Therefore, some saturation in the recovery traces (b) is pronounced for larger t_s.

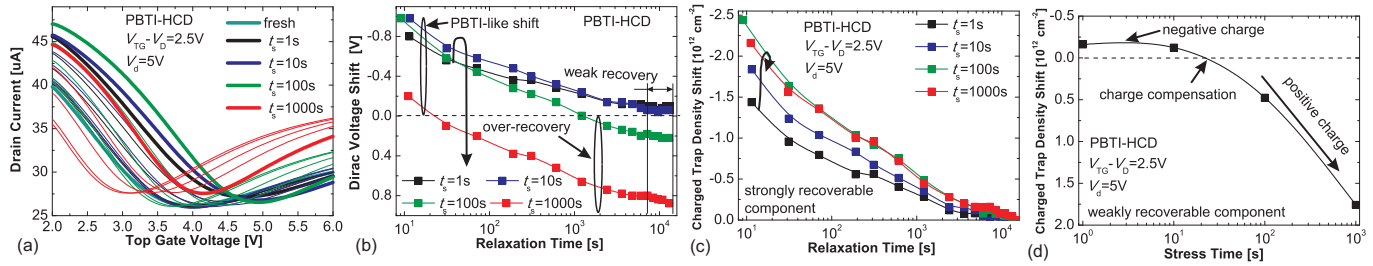

Fig. 6: a) Time evolution of the top gate transfer characteristics after PBTI-HCD stress with $V_{TG}-V_D=2.5$ V and $V_d=5$ V. b) The corresponding ΔV_D recovery traces demonstrate that the magnitude of PBTI-like degradation tends to decrease starting from $t_s=100$ s. At the same time, for larger t_s a recovery beyond the initial V_D (i.e. over-recovery) is observed. Although the strongly recoverable component (c) is completely associated with a relaxation of negative charge introduced by the bias contribution, at larger t_s it is suppressed by the HC contribution. However, the main impact of the HC contribution is associated with the weakly recoverable component (d). Contrary to Fig. 5, for larger t_s negative charge introduced by PBTI is completely compensated by positively charged defects associated with the dominant HC contribution. The presence of this extra positive charge explains the observed over-recovery.

the corresponding ΔV_D recovery traces contain both strongly and weakly recoverable components. The strongly recoverable component reflects a relaxation of negative charge introduced by PBTI. Since the PBTI contribution dominates over the HC one, the weakly recoverable component is also associated with negatively charged defects which leads to an incomplete recovery. However, for the largest t_s the HC contribution, which introduces positively charged defects, is strong enough to partially compensate the negative charge. Therefore, some signs of saturation are visible on the recovery traces for larger t_s. In Fig. 6 the related results for PBTI-HCD with smaller V_{TG} - V_D = 2.5 V are provided. Contrary to the previous case, the magnitude of the PBTI-like Dirac point shift decreases starting from $t_s=100$ s and becomes insignificant after the stress with $t_s=1000$ s. In addition, after the two longest stresses recovery proceeds towards left from the initial V_D, i.e. over-recovery is observed. Although the strongly recoverable component is still associated with a recovery of negatively charged defects, the contribution of PBTI to the weakly recoverable component is significantly smaller compared to Fig. 5. Therefore, the stress with larger t_s leads to a complete compensation of weakly recoverable negative charge and introduces some extra positively charged defects which are associated with the HC contribution. The presence of these defects is the origin of

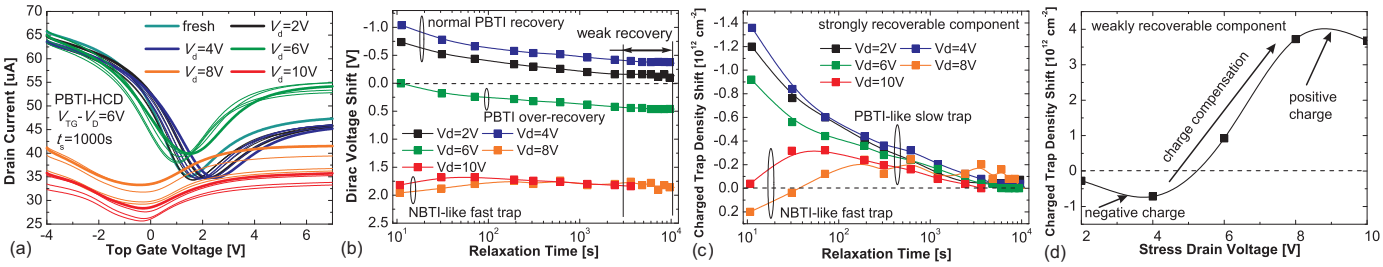

Fig. 7: a) Time evolution of the top gate transfer characteristics after PBTI-HCD stress with constant $t_s = 1000\,s$ and variable V_d. b) The corresponding recovery traces contain both strongly recoverable (c) and weakly recoverable (d) components. The two stresses with smaller V_d lead to a recoverable PBTI-like degradation. Since the HC contribution in that case is small, a weakly recoverable negative charge introduced by the PBTI contribution dominates. Therefore, an incomplete recovery is observed. The stress with $V_d = 6\,V$ is already strong enough to compensate the bias contribution and to reduce a PBTI-like shift. However, the Dirac point still recovers in a PBTI-like manner, which is associated with a relaxation of strongly recoverable negative charge introduced by the PBTI contribution. The recovery beyond the initial V_D (cf. Fig. 6) hints at an extra weakly recoverable positive charge which is introduced by the HC contribution. The two stresses with larger V_d lead to a purely NBTI-like degradation. The initial Dirac point shift is mainly contributed by the positively charged defects which are introduced by the HC contribution. Interestingly, some of them contribute the strongly recoverable component by introducing an NBTI-like fast trap response, while the others are weakly recoverable. Despite the dominant HC contribution, a PBTI-like slow trap response is also present in the recovery traces. This is associated with a relaxation of negatively charged defects induced by PBTI.

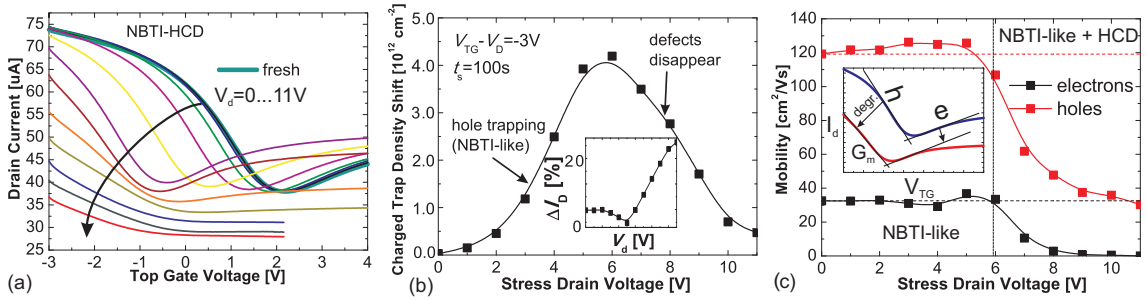

Fig. 8: a) Top gate transfer characteristics measured after subsequent NBTI-HCD stresses with different V_d. Acceleration of NBTI degradation by the HCD component leads to a charging of all defects after a stress with $V_d = 6\,V$. The subsequent stress cycles with larger V_d make some defects disappear (b) and result in an increase of the vertical drift ΔI_D (left inset). c) The mobility can be estimated using the transconductance G_m obtained as a slope of the linear parts of the I_d-V_{TG} curves (right inset). Both electron and hole mobility decrease after the stresses with a larger V_d (dashed lines are the mobilities of the unstressed device). However, the relative decrease in the electron mobility is more significant. This is because both HC and bias components of the applied stress introduce positively charged defects. Therefore, the electrons experience attractive scattering which is stronger than the repulsive scattering experienced by holes [16]. Despite the overal fraction of positively charged defects significantly decreases after the strongest stresses, a decrease in mobility allows to conclude that the defects situated more closely to the channel, which dominantly contribute to the mobility, remain stable. Moreover, a symmetric behaviour of mobilities hints at some contribution of neutral defects [16, 17] which can either be introduced by the stress or substitute disappearing positive charges.

the observed over-recovery. Interestingly, the difference in the magnitudes of the PBTI contributions in the two considered cases mainly impacts the weakly recoverable component, while the strongly recoverable component remain comparable.

In order to investigate the interplay between the defects of different signs in more detail, we apply subsequent stresses with a rather large PBTI contribution (V_{TG}-$V_D = 6\,V$) and different V_d for $t_s = 1000\,s$. The degradation/recovery dynamics are analyzed in Fig. 7. Clearly, the two stresses with smaller V_d lead to a PBTI-like degradation with incomplete recovery. This hints at domination of PBTI which introduces negatively charged defects and contributes both strongly and weakly recoverable components. After the stress with $V_d = 6\,V$ the PBTI-like shift of the Dirac point is not significant and some over-recovery is observed (cf. Fig. 6). This means that the strongly recoverable component is contributed by PBTI while the weakly recoverable component is associated with an extra positive charge introduced by the HC contribution. The stresses with the two largest V_d lead to a completely NBTI-like degradation. In that case the HC contribution creates both strongly and weakly recoverable positive charges. The former introduces an NBTI-like fast trap response which is similar to the one observed for pure NBTI [13] while the latter leads to an NBTI-like nature of the weakly recoverable component. At the same time, the bias contribution associated with PBTI-like relaxation of negatively charged defects is present after the fast trap has completely recovered (i.e. slow trap). Interestingly, the stress with $V_d = 8\,V$ causes a more significant NBTI-like ΔV_D than the one with $V_d = 10\,V$, likely due to disappearing defects (cf. Fig. 4).

In Fig. 8 the transformation of the top gate transfer characteristics after the subsequent NBTI-HCD stresses with increasing V_d is studied. After the stress with larger V_d the defects disappear, which is followed by a strong increase of the vertical drift ΔI_D and a change in the characteristics shape. The latter is associated with a degradation of mobility which can be estimated from the transcondactance G_m measured in the linear regions [18] (Fig. 8c). One can see that the stresses with smaller V_d does not significantly change the mobility which means that the created positively charged defects are situated at a considerable distance from the graphene channel. Although at larger V_d the overal concentration shift tends to decrease, both electron and hole mobility start to decrease significantly. Therefore, we can conclude that the defects situated closely

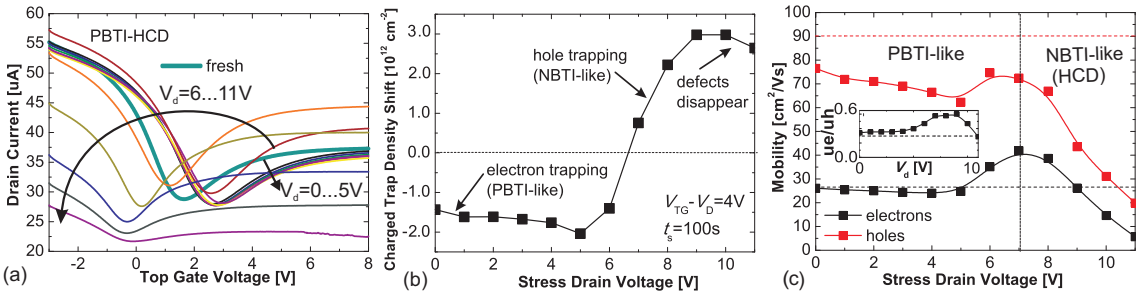

Fig. 9: a) Top gate transfer characteristics measured after subsequent PBTI-HCD stresses with different V_d. The PBTI-like degradation is pronounced only up to V_d=5 V. At larger V_d it is compensated by the strong HC contribution and then an NBTI-like degradation is observed. After all the defects have become charged, they tend to disappear (cf. Figs.4,7,8). b) All these features can be nicely depicted in terms of ΔN_T. c) The degradation of hole mobility is stronger after the stresses with smaller V_d, which is due to attractive scattering on negatively charged defects introduced by the PBTI contribution. However, during the transition from PBTI- to NBTI-like degradation the electron mobility considerably increases with respect to its initial value; the electron/hole mobility ratio also has a maximum (inset). This is because the charge compensation following this transition is accompained by screening effects [17] which make the potential field of some defects weaker. A considerable degradation of mobility starts only after the transition to an NBTI-like behavior. The presence of an extra positive charge introduced by the HC contribution makes a relative decrease in the electron mobility stronger, in agreement with [16].

to the channel are more stable and that their fraction still increases. At the same time, a relative decrease of electron mobility is stronger than for the hole mobility, which is because all the defects involved in scattering processes are positively charged. That is why the scattering of electrons is of attractive nature while the scattering of holes is repulsive. According to the attractive/repulsive scattering asymmetry reported in [16], the former is known to be stronger. However, some symmetry in the behaviour of electron and hole mobility hints at scattering on neutral defects which may also contribute the mobility [16, 17].

The related results for PBTI-HCD are provided in Fig. 9. After stress with smaller V_d the Dirac point is shifted in a PBTI-like manner due to trapping of electrons in the top gate oxide; the absolute value of negative ΔN_T increases (Fig. 9b). At moderate V_d ΔN_T changes sign which reflects the compensation of the PBTI component by HCD and a transition to NBTI-like behaviour. Further increase of V_d leads to an increase in positive ΔN_T. Once all the defects have become positively charged, ΔN_T tends to decrease. As in the previous case, the mobility degradation is consistent with an attractive/repulsive scattering asymmetry [16]. At smaller V_d the degradation of the hole mobility is stronger due to the presence of negatively charged defects, while at larger V_d additional positively charged defects lead to a more significant degradation of the electron mobility. However, charge compensation at moderate V_d leads to a significant increase of the electron mobility beyond its initial value. This is because the interplay between the defects of different signs is accompained by screening effects [17] which may reduce the potential field of some defects.

V. Conclusions

A first experimental observation of HCD in GFETs is reported. The impact of HCD consists in a shift of the Dirac point and a mobility change which are correlated and can be understood based on the previously reported attractive/repulsive scattering asymmetry. In contrast to Si technologies, HCD in GFETs is recoverable. At the same time, the dynamics of HCD and its recovery in GFETs strongly correlate with the top gate bias magnitude and polarity. Interestingly, the HC contribution can either accelerate or suppress the degradation.

VI. Acknowledgements

The authors thank the EC for the financial support through the STREP projects MoRV (619234) and GRADE (n° 317839), an ERC Starting Grant (InteGraDe, n° 307311), the German Research Foundation (DFG, LE 2440/1-1 and 2-1).

References

[1] A. Geim and K. Novoselov, "Numerical Methods for Semiconductor Device Simulation," *Nature Materials*, vol. 6, no. 3, pp. 183–191, 2007.
[2] V. Dorgan, M.-H. Bae, and E. Pop, "Mobility and Saturation Velocity in Graphene on SiO2," *Applied Physics Letters*, vol. 97, p. 082112, 2010.
[3] S. Vaziri, G. Lupina, A. Paussa, A. D. Smith, C. Henkel, G. Lippert, J. Dabrowski, W. Mehr, M. Östling, and M. Lemme, "A Manufacturable Process Integration Approach for Graphene Devices," *Solid-State Electron.*, vol. 84, pp. 185–190, 2013.
[4] K. Novoselov, A. Geim, S. Morozov, D. Jiang, Y. Zhang, S. Dubonos, I. Grigorieva, and A. Firsov, "Electric Fielld Effect in Atomically Thin Carbon Films," *Science*, no. 306, pp. 666–669, 2004.
[5] M. Lemme, T. Echtermeyer, M. Baus, and H. Kurz, "A Graphene Field Effect Device," *IEEE Electron Device Letters*, vol. 27, no. 4, pp. 1–12, 2007.
[6] S.-J. Han, Z. Chen, A. Bol, and Y. Sun, "Channel-Length-Dependent Transport Behaviors of Graphene Field-Effect Transistors," *IEEE Electron Device Lett.*, vol. 32, no. 6, pp. 812–814, 2011.
[7] M. Engel, M. Steiner, A. Lombardo, A. Ferrari, H. Loehneysen, P. Avouris, and R. Krupke, "Light-matter Interaction in a Microcavity-controlled Graphene Transistor," *Nature Communications*, vol. 3, pp. 1–6, 2012.
[8] S. Imam, S. Sabri, and T. Szkopek, "Low-Frequency Noise and Hysteresis in Graphene Field-Effect Transistors on Oxide," *Micro & Nano Letters*, vol. 5, no. 1, pp. 37–41, 2010.
[9] W. Liu, X. Sun, X. Tran, Z. Fang, Z. Wang, F. Wang, L. Wu, J. Zhang, J. Wei, H. Zhu, and H. Yu, "Observation of the Ambient Effect in BTI Characteristics of Back-Gated Single Layer Graphene Field Effect Transistors," *IEEE Trans.Electron Devices*, vol. 60, no. 8, pp. 2682–2686, 2013.
[10] Y. Illarionov, A. Smith, S. Vaziri, M. Ostling, T. Mueller, M. Lemme, and T. Grasser, "Bias-temperature Instability in Single-layer Graphene Field-effect Transistors: a Reliability Challenge," in *IEEE SNW*, 2014, pp. 29–30.
[11] S. Tyaginov, I. Starkov, H. Enichlmair, J. Park, C. Jungemann, and T. Grasser, "Physics-Based Hot-Carrier Degradation Models," *ECS Transactions*, pp. 321–352, 2011, .
[12] W. Liu, X. Sun, X. Tran, Z. Fang, Z. Wang, F. Wang, L. Wu, J. Zhang, J. Wei, H. Zhu, and H. Yu, "Vth Shift in Single-Layer Graphene Field-Effect Transistors and Its Correlation With Raman Inspection," *IEEE Trans. Device Mater. Reliab.*, vol. 12, no. 2, pp. 478 - 481, 2012.

[13] Y. Illarionov, A. Smith, S. Vaziri, M. Ostling, T. Mueller, M. Lemme, and T. Grasser, "Bias-Temperature Instability in Single-Layer Graphene Field-Effect Transistors," *Appl.Phys.Lett.*, vol. 105, p. 143507, 2014.
[14] T. Grasser, P.-J. Wagner, H. Reisinger, T. Aichinger, G. Pobegen, M. Nelhiebel, and B. Kaczer, "Analytic Modeling of the Bias Temperature Instability Using Capture/Emission Time Maps," in *IEDM*, Dec. 2011, pp. 27.4.1–27.4.4.
[15] M. D. Groeseneken, J. Zhang, Z. Ji, W. Zhang, B. Kaczer, S. De Gendt, and G., "Defect Loss: A New Concept for Reliability of MOSFETs," *IEEE Electron Device Lett.*, vol. 33, no. 4, pp. 480–482, 2012.
[16] D. Novikov, "Numbers of Donors and Acceptors from Transport Measurements in Graphene," *Appl.Phys.Lett.*, vol. 91, p. 102102, 2007.
[17] M. Katsnelson and K. Novoselov, "Graphene: New Bridge between Condensed Matter Physics and Quantum Electrodynamics," *Solid State Comm.*, vol. 143, pp. 3–13, 2007.
[18] G. Venugopal, K. Krishnamoorthy, and S. Kim, "Investigation of Transfer Characteristics of High Performance Graphene Flakes," *J. Nanoscience & Nanotechnology*, vol. 13, pp. 3515–3518, 2013.